Physics – Uspekhi **62** (3) 275 – 281 (2019)

CONFERENCES AND SYMPOSIA

PACS numbers: 63.20.kd, **71.70. – d**, 75.50.Ee, **75.85. + t**, 78.20.Bh, **78.30. – j**

New effects of the electron–phonon interaction in dielectrics (50th anniversary of the Institute of Spectroscopy, Russian Academy of Sciences)

M N Popova, K N Boldyrev

DOI: https://doi.org/10.3367/UFNe.2018.06.038413

Contents

Abstract. We have studied the electron–phonon interaction (EPI) in multiferroic $PrFe_3(BO_3)_4$ applying reflection methods in far-infrared (terahertz) spectral range and theoretical simulations. A specific feature of $PrFe_3(BO_3)_4$ is that the 4f-electron excitation of the Pr^{3+} ion falls into a range between the longitudinal (LO) and transverse (TO) phonon mode frequencies. Simultaneously, inversion of the electronic oscillator occurs: its LO frequency becomes smaller than the TO frequency. With lowering temperature, a coupled electron–phonon mode emerges, and a new effect is observed: the reststrahlen band corresponding to a nondegenerate phonon mode splits. Yet another effect caused by the EPI is the appearance of a gap in the spectrum of electronic excitations of a stoichiometric rare-earth easy-axis antiferromagnet placed into an arbitrarily weak external magnetic field directed along the easy magnetization axis.

Keywords: inverted electronic oscillator, electron–phonon interaction, coupled electron–phonon mode, bifurcations in a magnetic field, terahertz spectroscopy

1. Introduction

The electron–phonon interaction (EPI) is responsible for many fundamental phenomena in solids, such as conventional superconductivity, different types of the Jahn–Teller effect, the splitting of degenerate phonon modes in concentrated transition metal compounds in an external magnetic field, the delocalization of electronic states in the optical phonon energy region, and, as a result, the observed electronic Davydov splitting. The electron–phonon interaction plays an important role in ferroelectricity, thermal and electrical conductivity, and energy dissipation in electronic devices. Narrow zero-phonon lines in crystals are shifted and strongly broadened with increasing temperature mainly due to the EPI. This interaction is responsible for the relaxation of Stark levels of rare-earth (RE) ions in crystals and, therefore, for their lifetimes, which is, in particular, important for laser applications.

In the case of the resonance between a phonon and electronic excitation, the EPI leads to the formation of coupled electron–phonon modes, accompanied by energy renormalization and the appearance of new branches in the excitation spectrum [1–7]. A gap in the spectrum of elementary excitations due to the repulsion of dispersion branches of the electron and phonon subsystems (the so-called anticrossing effect) has been observed in various experiments with transition-metal compounds. In measuring Raman spectra and IR reflection experiments probing the Γ point ($\mathbf{k} = 0$) of the Brillouin zone, anticrossings and intensity transfer between components of coupled electron–phonon excitations were observed upon magnetic-field tuning the electron level to resonance with the phonon [1–3, 7, 8]. In neutron scattering experiments on $TmVO_4$ in a permanent magnetic field (determining the energy of the lowest Stark level of the Tm^{3+} ion), the anticrossing dispersion branches $\omega_1(\mathbf{k})$ and $\omega_2(\mathbf{k})$ were measured, and the dependence of the EPI on the wave vector $\mathbf{k}$ was studied [5].

Recently, we have observed in the IR reflection spectra of praseodymium ferroborate, $PrFe_3(BO_3)_4$, a number of new effects of this type caused by the EPI [9, 10]. Praseodymium ferroborate belongs to the family of new multiferroics with the general formula $RFe_3(BO_3)_4$ ($R = Pr - Er$, Y). These compounds have been extensively studied in recent years

M N Popova, K N Boldyrev
Institute of Spectroscopy, Russian Academy of Sciences,
ul. Fizicheskaya 5, 108840 Troitsk, Moscow, Russian Federation
E-mail: kn.boldyrev@gmail.com

Received 12 August 2018
Uspekhi Fizicheskikh Nauk **189** (3) 292 – 298 (2019)
DOI: https://doi.org/10.3367/UFNr.2018.06.038413
Translated by M Sapozhnikov; edited by A Radzig

due to their interesting physical properties and potential applications (see, for example, Refs [11–18]). The interactions among the charge, spin, and phonon systems play a key role in a variety of phases and phenomena observed in multiferroics [19, 20]. Whereas the spin–phonon interaction in multiferroics was studied, in particular, by optical methods [21–24], data on the interaction of electronic excitations with phonons in multiferroics were absent.

2. Crystal and magnetic structures, phonons, and 4f-electron excitations of praseodymium ferroborate

The $RFe_3(BO_3)_4$ ferroborates exhibit the noncentrosymmetric trigonal structure of a natural mineral huntite consisting of helical chains of FeO_6 octahedrons directed along the c-axis and connected by BO_3 triangles and distorted RO_6 prisms [25]. In the case of $RFe_3(BO_3)_4$ (R = Pr, Nd, Sm), the structure is described by the spatial $R32$ group at all temperatures [15–17 26, 27], with the primitive cell containing one formula unit, i.e., 20 atoms. Correspondingly, the phonon spectrum consists of 60 branches. Fifty-seven optical phonons of the Γ point are characterized by irreducible representations of the factor group 32 in the following way [15]: $\Gamma_{\rm vibr} = 7A_1 + 12A_2(z) + 19E(xy)$. The A_2 phonons are IR active for the $\mathbf{E} \parallel c$ polarization, and the E phonons are active for the $\mathbf{E} \perp c$ polarization. The E and A_1 modes are also Raman-active. The A_1 and A_2 phonons are nondegenerate, while the E phonons are doubly degenerate. The lowest-frequency phonon (45 $\rm cm^{-1}$ for $PrFe_3(BO_3)_4$) has the A_2 symmetry and is followed by the E phonon (84 $\rm cm^{-1}$).

The RE ion occupies one position with the 32 symmetry in the crystal lattice. The Stark levels of the non-Kramers ion (i.e., the ion with an even number of electrons, as in Pr^{3+}) are characterized by nondegenerate irreducible representations $\Gamma_1(A_1)$ and $\Gamma_2(A_2)$ and doubly degenerate representation $\Gamma_3(E)$ of the 32-symmetry point group (notations in parentheses are accepted in vibrational spectroscopy). $PrFe_3(BO_3)_4$ is ordered into the easy-axis antiferromagnetic (AFM) structure at $T_N = 32 \pm 1$ K [16, 17, 26]. The low-temperature magnetic and magnetoelectric properties of praseodymium ferroborate are mainly determined by the ground (Γ_2) and the first excited Γ_1 (with the energy close to 48 $\rm cm^{-1}$) singlet states of the Pr^{3+} ion [16–18, 26]. The next nearest Stark level is located at 192 $\rm cm^{-1}$ and has the symmetry of Γ_3 [16, 17].

The energy 48 $\rm cm^{-1}$ of the Stark level in praseodymium is close to the energy $\hbar\omega_0$ of the lowest-frequency IR-active A_2 phonon corresponding to displacements of the Pr^{3+} ion in the $PrFe_3(BO_3)_4$ crystal lattice [28]. Because the point symmetry group of the RE ion site coincides with the factor group of the space group of the crystal, we conclude immediately that the A_2 symmetry crystal vibrations can interact with electronic excitations appearing upon the $\Gamma_1 \leftrightarrow \Gamma_2$ transition. Thus, pronounced EPI effects in the far IR (terahertz) spectral region at about 50 $\rm cm^{-1}$ (1.5 THz) could be expected.

3. Investigation methods

A good optical quality $PrFe_3(BO_3)_4$ single crystal was grown by L N Bezmaternykh applying the solution–melt method at the Kirensky Institute of Physics, SB RAS (Krasnoyarsk). Details of the crystal growth are presented in Ref. [17]. The crystal was oriented by habitus using the optical polarization method. A crystal sample $5 \times 5 \times 10$ mm in size was prepared for conducting research.

Reflectance spectra were studied in the wave-number range from 20 to 100 $\rm cm^{-1}$ (0.6–3 THz) and in a broad temperature range from 4 to 300 K at the Institute of Spectroscopy, RAS (Troitsk, Moscow) with a Bruker IFS 125 HR Fourier spectrometer with a helium (4.2 K) bolometer detector and a closed-cycle Cryomech ST403 cryostat. In collaboration with two researchers T N Stanislavchuk and A A Sirenko of the Technological Institute in New Jersey (USA), reflectance spectra were also measured with a Bruker IFS-113v Fourier spectrometer at temperatures of 1.5–50 K in magnetic fields $\mathbf{B}_{\rm ext} \parallel c$ up to 8 T in the U41R line of the National Synchrotron Light Source at the Brookhaven National Laboratory (USA). Reflectance spectra in strong magnetic fields (up to 30 T) were also recorded at the High Field Magnet Laboratory (Nijmegen, The Netherlands) with the participation of Laboratory researcher D Kamensky.

4. Inverted electronic oscillator in the $PrFe_3(BO_3)_4$ reflection spectrum

The reflection spectra of $PrFe_3(BO_3)_4$ at several temperatures are shown at the top of Fig. 1, and the corresponding intensity maps with a smooth temperature scan are illustrated at the bottom panels. At room temperature, a strong reststrahlen band typical of an optical phonon was observed. The reflection spectrum in the $\mathbf{E} \parallel c$ polarization in a broad spectral region covering 12 A_2 modes was simulated based on the relationships

$$R = \left| \frac{\sqrt{\varepsilon} - 1}{\sqrt{\varepsilon} + 1} \right|^2 , \tag{1}$$

$$\varepsilon(\omega) = \varepsilon_\infty + \sum_i \frac{\Delta\varepsilon_i \omega_{0i}^2}{\omega_{0i}^2 - \omega^2 - {\rm i}\omega\gamma_i} , \tag{2}$$

where ω_{0i} is the TO frequency, γ_i is the decay constant, $\Delta\varepsilon_i$ is the oscillator strength of the ith transverse phonon mode, and ε_∞ is the high-frequency permittivity. This simulation gave the following parameters for the low-frequency A_2^1 phonon of interest for us at room temperature: $\omega_{\rm TO} \approx \omega_{01} \equiv \omega_0 = 44.6$ $\rm cm^{-1}$, $\omega_{\rm LO} = 58.8$ $\rm cm^{-1}$ (the frequencies of long-

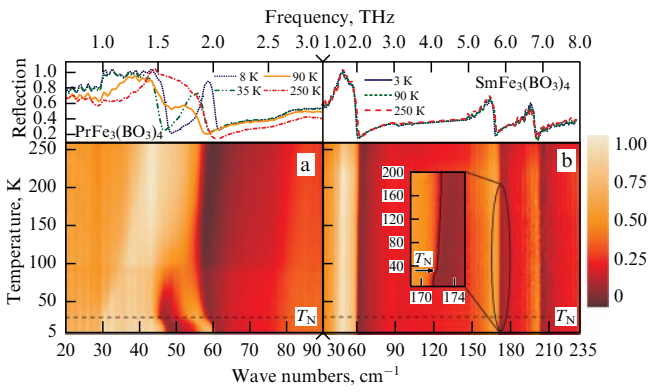

Figure 1. Reflection spectra taken in the $\mathbf{E} \parallel c$ polarization (top panels) and corresponding intensity maps (bottom panels) for (a) $PrFe_3(BO_3)_4$ and (b) $SmFe_3(BO_3)_4$. $T_N = 32 \pm 1$ K for both compounds. The splitting of the reststrahlen band in the $PrFe_3(BO_3)_4$ spectrum below ~ 100 K is clearly seen. The inset to Fig. 6 shows a step at T_N depending on $\omega(T)$ for the A_2^2 phonon mode in $SmFe_3(BO_3)_4$.

itudinal modes were found as zeroes of the function $\varepsilon(\omega)$), $\gamma = 2.8$ cm^{-1}, and $\Delta\varepsilon = 3.6$. These parameters are close to the corresponding ones for the isostructural $SmFe_3(BO_3)_4$ compound: $\omega_{TO} = 48.6$ cm^{-1}, $\omega_{LO} = 61.5$ cm^{-1}, $\gamma = 2.4$ cm^{-1}, and $\Delta\varepsilon = 2.9$. At a temperature of about 100 K, the splitting of the reststrahlen band in the $PrFe_3(BO_3)_4$ spectrum is observed. The components of the split band shift in opposite directions with a further temperature lowering and demonstrate a pronounced singularity at the magnetic ordering temperature T_N. On the contrary, the same phonon mode in $SmFe_3(BO_3)_4$ spectra barely changes with temperature. The dependences $\omega(T)$ for some modes exhibit a weak singularity at T_N (Fig. 1b) related to the spin–phonon interaction, as in the case of $EuFe_3(BO_3)_4$ compound studied earlier [24]. The only difference between the Sm and Pr compounds is that in $SmFe_3(BO_3)_4$ the 4f-electron excitation of the symmetry coinciding with that for the A_2^1 phonon with a frequency of about 50 cm^{-1} lies much higher (by 220 cm^{-1} [29]), whereas in $PrFe_3(BO_3)_4$ this excitation falls into the TO–LO range of this phonon. This is the decisive argument confirming the assumption that we observe in the $PrFe_3(BO_3)_4$ spectra the interaction between the phonon and 4f-electron excitation.

The splitting of reststrahlen bands was earlier observed in IR reflection spectra, when a comparatively weak vibration lay in the TO–LO range of a strong phonon of the same symmetry. Such a situation was first discussed by Scott and Porto [30] for the spectra of quartz. They noticed that the LO frequency of a weak mode proved to be *lower* than its TO frequency, i.e., an inversion of the TO and LO frequencies occurred. Other examples were pointed out in studies by Vinogradov [31] and Gervais and co-workers [32–35]. Later on Vinogradov and colleagues reported observation of inverted phonons in the IR reflection spectra of a family of $ZnSe_xS_{1-x}$ crystals for small x. In this case, the TO–LO frequency inversion occurs in the quasiresonance mode of impurity Se atoms in ZnS located inside the longitudinal–transverse splitting of the fundamental phonon of ZnS (see Ref. [36] and references cited therein).

Such TO–LO frequency inversion of a weak mode upon its falling into the longitudinal–transverse splitting region of a strong mode, where the real part of the crystal permittivity is negative, can be easily explained from the physical point of view. Assume that the oscillator strengths of strong (1) and weak (2) modes $\Delta\varepsilon_1$ and $\Delta\varepsilon_2$ satisfy the inequality $\Delta\varepsilon_2 \ll \Delta\varepsilon_1$. In this case, the negative permittivity ε_1' produced by mode 1 in the $TO_2 - LO_2$ splitting region of mode 2 can be considered approximately constant and, disregarding the decay and from the condition of the function $\varepsilon(\omega)$ vanishing, the expression for ω_{LO_2} can be written out in the form

$$\omega_{TO_2}^2 - \omega_{LO_2}^2 \approx -\frac{\Delta\varepsilon_2 \omega_{TO_2}^2}{\varepsilon_1'} . \qquad (3)$$

Because the quantity ε_1' is negative in the frequency interval between ω_{TO_1} and ω_{LO_1}, we conclude that the LO_2 frequency of the weak mode is smaller than its TO_2 frequency (the *inverted* phonon). This point was considered in more detail in theoretical paper by Gervais [37], where the weak phonon frequency was gradually changed, intersecting the TO–LO interval of the strong mode.

For $PrFe_3(BO_3)_4$, we have mathematically the same situation: a strong (phonon) mode with the oscillator strength $\Delta\varepsilon_{ph}$ produces a negative permittivity in its TO–LO splitting region and a weak (electronic) oscillator with $\Delta\varepsilon_{el} \ll \Delta\varepsilon_{ph}$ is inverted, entering the TO–LO interval of the strong phonon. This study is the first observation of an inverted *electronic* oscillator.

5. Coupled electron–phonon mode in $PrFe_3(BO_3)_4$

The increase in the electron–phonon interaction with decreasing temperature results in the formation of a coupled electron–phonon mode and the redistribution of oscillator strengths between its quasiphonon and quasielectronic components. Figure 2 presents the dependences $\omega_{TO}(T)$ and $\omega_{LO}(T)$ for the quasiphonon A_2^1 and quasielectronic modes obtained from analyzing c-polarized reflection spectra. For comparison, the inset shows the temperature dependences of the TO and LO frequencies of the A_2^1 mode in $SmFe_3(BO_3)_4$. No singularities in their behavior, as in the behavior of the next-in-frequency doubly degenerate phonon E mode (Fig. 2), were observed.

We simulated a coupled electron–phonon mode using the theory developed in [4]. The frequencies of coupled excitations were found as roots of the equation

$$\omega^2 - \omega_{ph}^2 - \frac{2\omega_{ph}\omega_{el}(n_0 - n)|W|^2}{\omega^2 - \omega_{el}^2} = 0 , \qquad (4)$$

where ω_{ph} and ω_{el} are the phonon and electronic frequencies (in cm^{-1}), respectively, in the absence of interaction, n_0 and n are the relative populations of the ground and excited Stark states, respectively, and W is the EPI constant. This constant determines the change in the RE ion energy caused by the crystal field (CF) modulation with the vibrations. In the case of the A_2^1 phonon we are interested in and electronic excitation corresponding to the transition from the $|\Gamma_2\rangle$ ground state of the Pr^{3+} ion to the first excited $|\Gamma_1\rangle$ state, this constant can be written out in the form [8]

$$W \equiv W_{12}(A_2^1) = \langle\Gamma_1|\bar{B}_3^4 O_3^4 + \bar{B}_3^6 O_3^6 + \bar{B}_{-6}^6 O_{-6}^6|\Gamma_2\rangle = W_0 \exp(i\eta) . \qquad (5)$$

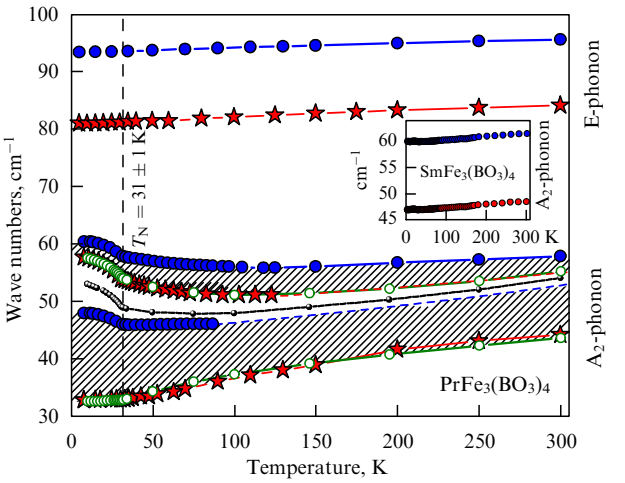

Figure 2. (Color online.) Temperature dependences of the TO (red asterisks) and LO (blue circles) frequencies obtained from the IR reflection spectra of $PrFe_3(BO_3)_4$ and $SmFe_3(BO_3)_4$ (inset). Dots show positions of the Stark level of Pr^{3+} found from optical spectra [16, 17]. The TO frequencies of coupled electron–phonon modes calculated from formula (6) are shown by unfilled circles connected with thick green lines.

Here, O_q^p are Stevens operators of the Γ_2 symmetry (or A_2 in the notation accepted for phonons), and $\bar{B}_q^p = \bar{B}_q^p(A_2^1)$ are the constants describing interaction of the Pr^{3+} ion in $PrFe_3(BO_3)_4$ with the optical A_2^1 phonon of the point Γ. They can be calculated as derivatives of the crystal-field parameters with respect to ion displacements in the given phonon mode [8]. The solution of equation (4) gives the frequencies of coupled electron–phonon modes:

$$\omega_{\pm}^2 = \frac{\omega_{ph}^2 + \omega_{el}^2}{2} \pm \sqrt{\frac{(\omega_{el}^2 - \omega_{ph}^2)^2}{4} + 2\omega_{ph}\omega_{el}(n_0 - n)\,|W|^2}\,. \quad (6)$$

At high temperatures, when $n \approx n_0$ the EPI vanishes and we have purely phonon and electronic excitations with frequencies $\omega_+ = \omega_{el}$ and $\omega_- = \omega_{ph}$, respectively.

We will simulate experimental data in Fig. 2 using relation (6). In the case of the Boltzmann distribution of electronic-level population, one finds $n_0 - n = \tanh(\omega_{el}(T)/2kT)$. The function $\omega_{el}(T)$ is the temperature-dependent position of the Stark level of the Pr^{3+} ion, determined earlier from optical spectra [16, 17]. The interaction constant W defined by relation (5) can depend on temperature below T_N because of the mixing of the $|\Gamma_1\rangle$ and $|\Gamma_2\rangle$ states by the internal magnetic field $B_{int}(T)$ produced by the ordered magnetic moments of Fe atoms. By ignoring the higher electronic states, we arrive at the following relation [38]

$$W^2(T) = W_0^2\left[1 - \frac{2|\alpha(T)|^2(\cos 2\varphi + 1)}{(1 + |\alpha(T)|^2)^2}\right]. \quad (7)$$

Here, W_0 is the interaction constant in the paramagnetic phase of $PrFe_3(BO_3)_4$, $\alpha(T) = V_{12}(T)/\omega_{12}(T_N)$, where

$$V_{12}(T) = \mu_B g_0 B_{ex}(T)\langle\Gamma_1|J_z|\Gamma_2\rangle = V_0 \exp(i\zeta) \quad (8)$$

is the matrix element of the Zeeman interaction (μ_B is the Bohr magneton, and g_0 is the Landé factor) and $\varphi = \eta - \zeta$. The previously calculated matrix element $\langle\Gamma_1|J_z|\Gamma_2\rangle$ is a real quantity [16, 17], which means that $\zeta = 0$. It follows from symmetry considerations with respect to the time reversal and comparison of relations (8) and (5) that W is a purely imaginary quantity and $\eta = \pi/2$. Thus, $2\varphi = \pi$ and, according to formula (7), the mixing of the $|\Gamma_1\rangle$ and $|\Gamma_2\rangle$ states by the internal magnetic field below temperature T_N does not affect the EPI constant in the case of interest for us.

The interaction constant W_0 and the initial phonon frequency ω_{ph} at 300 K were varied to obtain the best fit of experimental data. In addition, we introduced the linear in temperature shift of ω_{ph} independent of the EPI, the same as that for the isostructural $SmFe_3(BO_3)_4$ compound (see the inset to Fig. 2). The dependences calculated by expression (6) with parameters $W_0 = 14.6\ cm^{-1}$ and $\omega_0 = 45.5\ cm^{-1}$ are presented in Fig. 2. They are in good agreement with experimental temperature dependences of the TO frequencies.

Thus, two bands at frequencies of about $50\ cm^{-1}$ in the IR reflection spectrum of $PrFe_3(BO_3)_4$ correspond to the two branches of the coupled 4f electron–phonon mode formed below the temperature of ~ 100 K at which the population of the first excited Stark level of the Pr^{3+} ion noticeably decreases. As temperature is lowered, the high-frequency quasielectronic branch borrows the intensity from the low-frequency quasiphonon branch. Notice that pure 4f-electron excitations are not observed in reflection spectra, because of the low oscillator strength ($\sim 10^{-6} - 10^{-8}$).

6. Coupled electron–phonon mode of $PrFe_3(BO_3)_4$ in a magnetic field. Bifurcation points

The formation of coupled electron–phonon modes causes noticeable changes in the low-energy part of the crystal spectrum determining the thermodynamic and magnetic properties of the compound. Therefore, it is important to understand, in particular, the behavior of coupled modes in external magnetic fields.

Figures 3a, c show the reflection spectra of a $PrFe_3(BO_3)_4$ crystal in magnetic fields $\mathbf{B}_{ext} \parallel c$ up to 8 T at temperatures of about 1.5 K (Fig. 3a) and 40 K $> T_N = 32$ K (Fig. 3c). The corresponding intensity maps are presented in Figs 3b, d. In the easy-axis AFM phase ($T = 1.5$ K, $B_{ext} < B_{SF}$) (the subscript is related to the spin-flop transition), the magnetic moments of iron directed along the c-axis produce an internal alternating field $\mathbf{B}_{int} \parallel c$ on praseodymium ions, reaching $B_{int} \approx 10.5$ T at 1.5 K [16, 17]. The external magnetic field $\mathbf{B}_{ext} \parallel c$ is vectorially added to this field so that half the Pr^{3+}

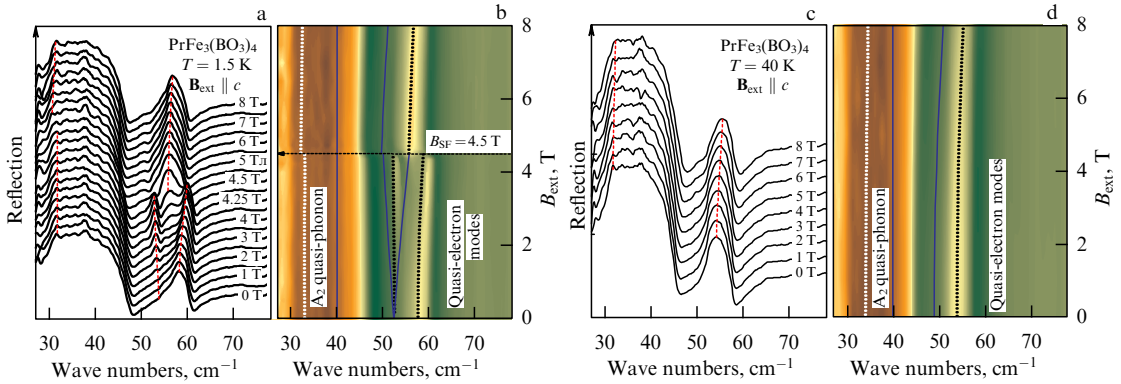

Figure 3. (Color online.) Reflection spectra of the $PrFe_3(BO_3)_4$ crystal in the $\mathbf{E} \parallel c$ polarization in magnetic fields $\mathbf{B}_{ext} \parallel c$, and corresponding intensity maps in the frequency–magnetic field coordinates for (a, b) $T = 1.5$ K and (c, d) $T = 40$ K. Spectra at 1.5 K exhibit a spin-flop transition in the field $B_{SF} \approx 4.5$ T. Solid blue lines in figures (b, d) show the behavior of the phonon and two electronic branches in the absence of the EPI. Dotted lines are calculated from formulas (9) and (10) with the following set of parameters: (a–c) $|W| = 14.8\ cm^{-1}$, $\omega_{ph} = 40\ cm^{-1}$, $E = 49\ cm^{-1}$, $g_0\langle\Gamma_1|J_z|\Gamma_2\rangle = 1.9$, and (a, b) $B_{int} = 10.5$ T for $B_{ext} < B_{SF}$ (see text).

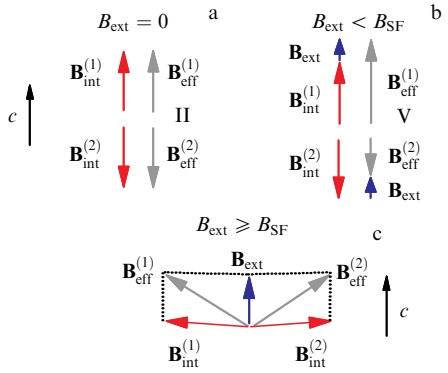

Figure 4. Schematic formation of the effective magnetic field for two praseodymium subsystems in different regions of the $B-T$ phase diagram in the case of $\mathbf{B}_{ext} \parallel c$: (a) AFM phase, $B_{ext} = 0$; (b) AMF phase, $B_{ext} < B_{SF}$ and (c) spin-flop phase, $B_{ext} \geqslant B_{SF}$.

ions 'feels' the effective field $B_{eff}^{(1)} = B_{int} + B_{ext}$ (Pr subsystem 1), while the other half feels the field $B_{eff}^{(2)} = B_{int} - B_{ext}$ (Pr subsystem 2), as shown schematically in Fig. 4b. In the absence of the EPI, two electronic branches exist with energies $\omega_{el,1}$ and $\omega_{el,2}$, corresponding to these two subsystems of praseodymium:

$$\omega_{el,i}^2 = E^2 + 4\mu_B^2 g_0^2 \left|\langle\Gamma_1|J_z|\Gamma_2\rangle\right|^2 \left|B_{eff}^{(i)}\right|^2, \quad i = 1, 2; \qquad (9)$$

here, $E = 49$ cm^{-1} is the energy of the first excited Stark level Γ_1 of the Pr^{3+} ion in paramagnetic praseodymium ferroborate. These branches are shown by solid blue lines in Fig. 3b. Their energies converge to the same value of ω_{el} for $B_{ext} \to 0$, $\omega_{el}^2 = E^2 + 4\mu_B g_0^2 |\langle\Gamma_1|J_z|\Gamma_2\rangle|^2 B_{int}^2$. One can see from Figs 3a, b that the two electronic branches observed in experiments in the region from 50 to 60 cm^{-1} converge to different values as $B_{ext} \to 0$, and a gap appears between them in an arbitrarily small magnetic field. Such a behavior is caused by the electron–phonon interaction.

To find the frequencies of coupled electron–phonon modes in the case of interaction of a nondegenerate phonon mode at the unperturbed frequency ω_{ph} with two electronic excitations at frequencies $\omega_{el,1}$ and $\omega_{el,2}$, we will write down an equation similar to Eqn (4) for the case of interaction with one electronic excitation:

$$(\omega^2 - \omega_{ph}^2) - 2\omega_{ph}|W|^2 \left(\frac{\omega_{el,1}(n_{01} - n_1)}{\omega^2 - \omega_{el,1}^2} + \frac{\omega_{el,2}(n_{02} - n_2)}{\omega^2 - \omega_{el,2}^2}\right) = 0. \qquad (10)$$

Here, n_{0i} and n_i are relative populations of the ground and first excited states, respectively, of the Pr^{3+} ion in the ith Pr subsystem, $i = 1, 2$. In our case of $T = 1.5$ K, $n_1 \approx n_2 \approx 0$, while $n_{01} \approx n_{02} \approx 1/2$. Then, equation (10) can be written out in the form

$$(x - x_{ph}) = \sqrt{x_{ph}}|W|^2 \left(\frac{\sqrt{x_{el,1}}}{x - x_{el,1}} + \frac{\sqrt{x_{el,2}}}{x - x_{el,2}}\right), \qquad (11)$$

where the notations $x_{ph} \equiv \omega_{ph}^2$, $x_{el,i} \equiv \omega_{el,i}^2$ are introduced. Figure 5 plots the graphic solution of equation (11). The right-hand part of the equation as a function of x consists of three branches 0, *1*, and *2* in Fig. 5 with singularities at points $x_{el,1}$ and $x_{el,2}$. These branches intersect with the straight line representing the left-hand part of equation (11) at three points

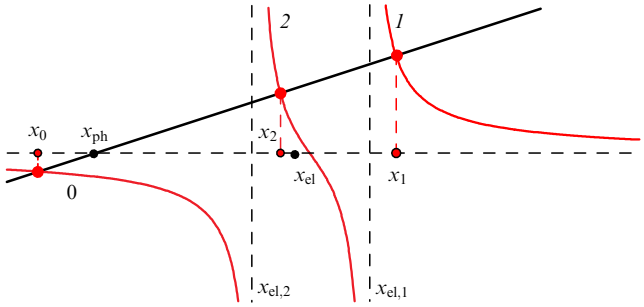

Figure 5. Graphic solution of equation (11). The roots of the equation are abscissas of the intersection points of the straight line and branches 0, 1, and 2. Branch 2 vanishes in the case of $x_{el,1} = x_{el,2}$, $x_{el} \equiv \omega_{el}^2 = E^2 + 4\mu_B g_0^2 |\langle\Gamma_1|J_z|\Gamma_2\rangle|^2 B_{int}^2$. Notation is presented in the text.

x_0, x_1, and x_2, which are the roots of equation (11). Branch *2* vanishes when $x_{el,1} = x_{el,2}$, and cubic equation (11) becomes quadratic. In our experiments with $PrFe_3(BO_3)_4$, three cases correspond to this situation: (1) the AFM phase, $B_{ext} = 0$, (2) the paramagnetic phase ($B_{int} = 0$) with any B_{ext}, and (3) the AFM spin–flop phase, $B_{ext} \geqslant B_{SF}$.

The first case was already considered in Section 5 of this paper. In the second case of the paramagnetic $PrFe_3(BO_3)_4$ crystal ($T = 40$ K, $B_{int} = 0$; see Figs 3c, d), the external magnetic field $\mathbf{B}_{ext} \parallel c$ shifts the excited Stark level Γ_1 upward, $\omega_{el}^2 = E^2 + 4\mu_B^2 g_0^2 |\langle\Gamma_1|J_z|\Gamma_2\rangle|^2 B_{ext}^2$, due to the nondiagonal Zeeman interaction with the ground Γ_2 level. A corresponding shift of both branches of the electron–phonon mode is observed. We simulated this behavior using the same approach as in the first case, with the same set of parameters ($|W| = 14.8$ cm^{-1}, $\omega_{ph}(40\text{ K}) = 40$ cm^{-1}, and $E = \omega_{el}(40\text{ K},\ B_{ext} = 0) = 49$ cm^{-1}). The results are shown by dotted lines in Figs 3c, d.

In the third case covering the antiferromagnetic $PrFe_3(BO_3)_4$ crystal placed in the external magnetic field $\mathbf{B}_{ext} \parallel c$ with the value $B_{ext} \geqslant B_{SF} = 4.5$ T ($T = 1.5$ K), the main component of the internal magnetic field of the Fe subsystem lies in the *ab* plane (see Fig. 4c) and does not affect the Pr subsystem (because the matrix elements of operators J_x and J_y between the states Γ_1 and Γ_2 of the Pr^{3+} ion are zero). The z-component of the internal magnetic field, as follows from estimates of the data on magnetization measurements [26], is much smaller than B_{ext} in the interval between B_{SF} and 30 T. Therefore, the behavior of Pr^{3+} ions in the spin-flop phase is determined by the external field $\mathbf{B}_{ext} \parallel c$. The field behavior of frequencies in the coupled electron–phonon mode of $PrFe_3(BO_3)_4$ ($T = 1.5$ K) in the external magnetic field $\mathbf{B}_{ext} \parallel c$ from 4.5 to 22 T is demonstrated in Figs 3a, b and 6a. When the magnetic field increases, the energy difference between the electronic level and the phonon also increases, the interaction between electronic and phonon excitations weakens, and the quasielectronic mode borrows progressively the smaller intensity from the quasi-phonon mode until its complete vanishing in the field of 22 T (see Fig. 6a). A weak trace of the quasielectronic mode appears again in the field of ~ 25 T, when this mode approaches the lowest-frequency phonon E mode (Fig. 6b). A weak interaction between these two excitations occurs because of admixture to the wave functions of the Γ_1 level the wave functions of the Γ_3 level at 192 cm^{-1} by the *ab*-component of the internal magnetic field on the Pr^{3+} ions in the spin-flop phase. The magnetic structure of the compound does not change in the range of

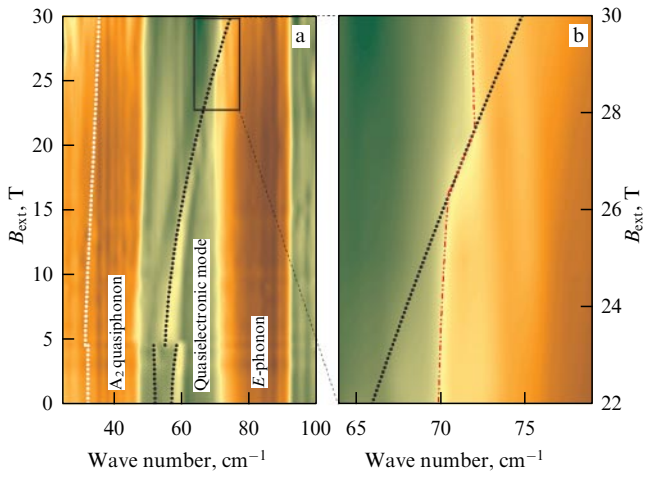

Figure 6. (a) Intensity map of the IR reflection of nonpolarized light by the $PrFe_3(BO_3)_4$ crystal in external fields $\mathbf{B}_{ext} \| c$ up to 30 T at $T = 1.5$ K. Dotted lines were calculated from formulas (9) and (120) with a following srt of parameters: $|W| = 14.8$ cm^{-1}, $E = 49$ cm^{-1}, $\omega_{ph} = 40$ cm^{-1}, and $g_0\langle\Gamma_1|J_z|\Gamma_2\rangle = 1.9$. (b) Magnified portion in the region of the TO frequency of the E-phonon in the field of 22–30 T. The dash-dotted line traces the TO-phonon frequency.

magnetic fields $B_{SF} < B_{ext} < 30$ T weaker than the Fe–Fe exchange field $B_{Fe-Fe} \sim 100$ T [18]. Notice that the same EPI constant $|W| = 14.8$ cm^{-1} operates in a broad range of magnetic fields from zero to 30 T. Experiments carried out in fields up to 30 T gave the exact value of the matrix element $\langle\Gamma_1|J_z|\Gamma_2\rangle$, providing the best fit of experimental data by the value of $g_0\langle\Gamma_1|J_z|\Gamma_2\rangle = 1.9$.

In the case of the EPI in an easy-axis antiferromagnet placed in an external magnetic field directed along the easy magnetic axis, the excitation spectrum contains two bifurcation points, as shown in Figs 3a, b. The first of them corresponds to the application of the field $B_{ext} \neq 0$, immediately converting the quadratic equation for the coupled electron–phonon mode to the cubic equation. A new excitation with frequency $\omega_2^2 \equiv x_2 < x_{el} \equiv \omega_{el}^2 = E^2 + 4\mu_B^2 g_0^2 |\langle\Gamma_1|J_z|\Gamma_2\rangle|^2 B_{int}^2$ appears in the spectrum. When $B_{ext} \to 0$, we have $x_2 \to x_{el}$, whereas the root x_1, which existed at $B_{ext} = 0$, tends to $x_{el} + O(|W|)$, so that $x_1 > x_{el}$ for any $|W| \neq 0$. Thus, for any $|W| \neq 0$ and $0 < B_{ext} < B_{SF}$, the spectrum of a coupled mode in the easy-axis AFM phase of $PrFe_3(BO_3)_4$ has two quasielectronic branches with *a gap between them*.

The second bifurcation point is observed for B_{SF}. When B_{ext} becomes lower than B_{SF}, the quadratic equation ((11) with $\omega_{el,1} = \omega_{el,2}$) transforms into the cubic equation ((11) with $\omega_{el,1} \neq \omega_{el,2}$), and one quasielectronic excitation splits into two excitations accompanied by a drastic frequency jump.

7. Conclusions

We have studied the electron–phonon interaction in a $PrFe_3(BO_3)_4$ multiferroic by the methods of far-IR (terahertz) reflection and theoretical simulations. For comparison, we also investigated an isostructural $SmFe_3(BO_3)_4$ crystal. A specific feature of the $PrFe_3(BO_3)_4$ compound is that the 4f-electron excitation of the Pr^{3+} ion, corresponding to the transition to the first excited Stark level in the Pr^{3+} ion, falls into the optical region between the TO- and LO-phonon frequencies of the same symmetry as the electronic excitation. In this case, the electronic oscillator is inverted so that its LO frequency becomes smaller than the TO frequency. Our study is the first observation of an inverted electronic oscillator. We have demonstrated the pronounced spectroscopic manifestations of the temperature-dependent electron–phonon interaction. In particular, a new effect of splitting the reststrahlen band corresponding to the nondegenerate phonon mode was observed. This effect is caused by the formation of a coupled electron–phonon mode. The EPI constant was found by simulations. Its comparatively large value (about 15 cm^{-1}) demonstrates the considerable role of the EPI in the physics of mutiferroics.

The study of the behavior of the coupled electron–phonon mode in an external magnetic field has revealed another new effect caused by the EPI, namely, the existence of a gap in the electronic spectrum of the easy-axis antiferromagnet in an arbitrarily weak external magnetic field directed along the easy axis of magnetization. As a result, the field behavior of the excitation spectrum qualitatively differs from that in the absence of the EPI.

Notice in conclusion that our study demonstrates new nontrivial manifestations of the electron–phonon interaction in solids and explains them with the aid of a comparatively simple model.

Acknowledgments

We are thankful to E A Vinogradov, B Z Malkin, and A V Popov for the fruitful discussions. K N B acknowledges a support of the Russian Foundation for Basic Research (grant Í 18-32-20142).

References

1. Dahl M, Schaack G *Phys. Rev. Lett.* **56** 232 (1986)
2. Kupchikov A K et al. *Sov. Phys. Solid State* **29** 1913 (1987); *Fiz. Tverd. Tela* **29** 3335 (1987)
3. Kraus J et al. *Z. Phys. B* **74** 247 (1989)
4. Kupchikov A K et al. *Sov. Phys. Solid State* **24** 1348 (1982); *Fiz. Tverd. Tela* **24** 2373 (1982)
5. Kjems J K, Hayes W, Smith S H *Phys. Rev. Lett.* **35** 1089 (1975)
6. Fennell T et al. *Phys. Rev. Lett.* **112** 017203 (2014)
7. Brinzari T V et al. *Phys. Rev. Lett.* **111** 047202 (2013)
8. Kupchikov A K et al., in *Spektroskopiya Kristallov* (Spectroscopy of Crystals) (Ed. A A Kaplyanskii) (Leningrad: Nauka, 1989) p. 85
9. Boldyrev K N et al. *Phys. Rev. B* **90** 121101(R) (2014)
10. Boldyrev K N et al. *Phys. Rev. Lett.* **118** 167203 (2017)
11. Yen F et al. *Phys. Rev. B* **73** 054435 (2006)
12. Chaudhury R P et al. *Phys. Rev. B* **80** 104424 (2009)
13. Adem U et al. *Phys. Rev. B* **82** 064406 (2010)
14. Popov A I, Plokhov D I, Zvezdin A K *Phys. Rev. B* **87** 024413 (2013)
15. Fausti D et al. *Phys. Rev. B* **74** 024403 (2006)
16. Popova M N et al. *Phys. Rev. Lett.* **102** 187403 (2009)
17. Popova M N et al. *Phys. Rev. B* **80** 195101 (2009)
18. Kostyuchenko N V, Popov A I, Zvezdin A K *Phys. Solid State* **54** 1591 (2012); *Fiz. Tverd. Tela* **54** 1493 (2012)
19. Cheong S-W, Mostovoy M *Nature Mater.* **6** 13 (2007)
20. van den Brink J, Khomskii D I *J. Phys. Condens. Matter* **20** 434217 (2008)
21. Haumont R et al. *Phys. Rev. B* **73** 132101 (2006)
22. Kang T D et al. *Phys. Rev. B* **82** 014414 (2010)
23. Bhadram V S et al. *Europhys. Lett.* **101** 17008 (2013)
24. Boldyrev K N et al. *Phys. Lett. A* **376** 2562 (2012)
25. Leonyuk N I, Leonyuk L I *Prog. Cryst. Growth Charact. Mater.* **31** 179 (1995)
26. Kadomtseva A M et al. *JETP Lett.* **87** 39 (2008); *Pis'ma Zh. Eksp. Teor. Fiz.* **87** 45 (2008)
27. Chukalina E P et al. *Phys. Lett. A* **374** 1790 (2010)

28. Chernyshev V A et al. *Phys. Solid State* **58** 1642 (2016); *Fiz. Tverd. Tela* **58** 1587 (2016)
29. Popova M N et al. *JETP* **118** 111 (2014); *Zh. Eksp. Teor. Fiz.* **145** 128 (2014)
30. Scott J F, Porto S P S *Phys. Rev.* **161** 903 (1967)
31. Vinogradov E A "Issledovanie opticheskikh fononov v poluprovodnikovykh soedineniyakh A^2B^6" ("Study of optical phonons in A^2B^6 semiconductors"), Ph.D. Thesis (Phys.-Math.) (Dolgoprudnyi: Moscow Institute of Physics and Technology, 1973)
32. Gervais F, Piriou B, Cabannes F *Phys. Status Solidi B* **55** 143 (1973)
33. Gervais F, Piriou B *J. Phys. C* **7** 2374 (1974)
34. Gervais F, Piriou B *Phys. Rev. B* **10** 1642 (1974)
35. Gervais F, Piriou B *Phys. Rev. B* **11** 3944 (1975)
36. Vinogradov E A et al. *Phys. Usp.* **52** 290 (2009); *Usp. Fiz. Nauk* **179** 313 (2009)
37. Gervais F *Opt. Commun.* **22** 116 (1977)
38. Landau L D, Lifshitz E M *Quantum Mechanics. Non-Relativistic Theory* (Oxford: Pergamon Press, 1965); Translated from Russian: *Kvantovaya Mekhanika. Nerelyativistskaya Teoriya* (Moscow: Fizmatlit, 1963)